

---

# Rethinking Metrics and Benchmarks of Video Anomaly Detection

---

**Zihao Liu**

Communication University of China  
liuzihao@cuc.edu.cn

**Xiaoyu Wu\***

Communication University of China  
wuxiaoyu@cuc.edu.cn

**Wenna Li**

Communication University of China  
liwenna@cuc.edu.cn

**Linlin Yang**

Communication University of China  
mu4yang@gmail.com

## Abstract

Video Anomaly Detection (VAD), which aims to detect anomalies that deviate from expectation, has attracted increasing attention in recent years. Existing advancements in VAD primarily focus on model architectures and training strategies, while devoting insufficient attention to evaluation metrics and benchmarks. In this paper, we rethink VAD evaluation protocols through comprehensive experimental analyses, revealing three critical limitations in current practices: 1) existing metrics are significantly influenced by single annotation bias; 2) current metrics fail to reward early detection of anomalies; 3) available benchmarks lack the capability to evaluate scene overfitting. To address these limitations, we propose three novel evaluation methods: first, we establish averaged AUC/AP metrics over multi-round annotations to mitigate single annotation bias; second, we develop a Latency-aware Average Precision (LaAP) metric that rewards early and accurate anomaly detection; and finally, we introduce two hard normal benchmarks (UCF-HN, MSAD-HN) with videos specifically designed to evaluate scene overfitting. We report performance comparisons of ten state-of-the-art VAD approaches using our proposed evaluation methods, providing novel perspectives for future VAD model development. Anonymous links for data and code are provided.

## 1 Introduction

Video Anomaly Detection (VAD) aims to identify abnormal frames deviating from expectations in video sequences, playing a pivotal role in applications such as intelligent surveillance, traffic management, and healthcare [1, 2]. In recent years, this task has garnered increasing attention, with existing methods [3–12] achieving satisfactory performance on several large-scale datasets [13–15] through weakly-supervised paradigms. Similar to other domains in machine learning, the advancement of VAD correlates with evaluation metrics and datasets. Despite its importance, this direction remains understudied. Inspired by similar studies in other domains [16, 17], we conduct a comprehensive analysis of the methods of evaluating VAD algorithms. Our investigation reveals that existing metrics and benchmarks fail to reliably and comprehensively evaluate VAD algorithms. We summarize the limitations in terms of annotation, metric, and benchmarking data as follows.

For annotation, existing evaluation methods are generally limited to leveraging single-round annotations, where each video is annotated only once. However, as illustrated in Figure 1(a), individual annotations may exhibit bias - one tends to favor the most salient abnormal behavior frames while

---

\*Corresponding Author

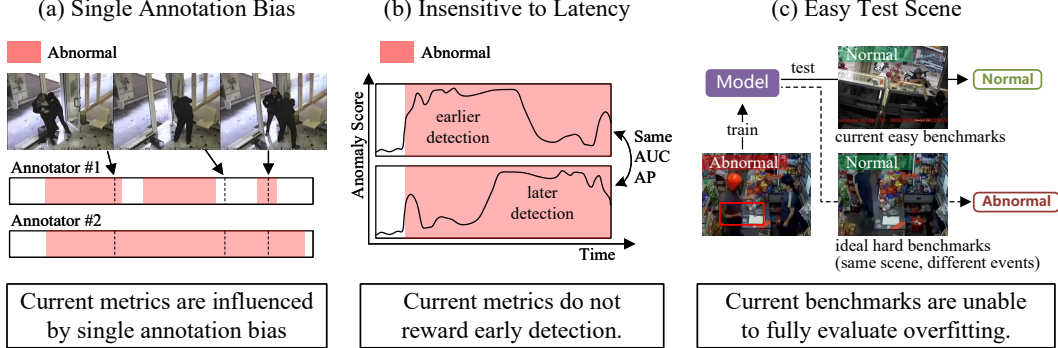


Figure 1: Three limitations in current metrics and benchmarks of video anomaly detection.

the other may favor more comprehensive event segments. The discrepancy of annotations could compromise the reliability of metric computations. [18] preliminarily reveals this phenomenon in the UCF-Crime dataset [13] by providing an alternative annotation. Some works [19, 20] also mention the label noise in UCF-Crime. However, these works lack systematic dataset analysis and focus exclusively on one dataset.

For metric design, the most commonly used metrics in VAD are AUC (Area Under receiver operating characteristic Curve) and AP (Average Precision). These metrics treat VAD as a frame-wise binary classification task, which is insensitive to the temporal position of predictions. In safety-critical applications such as emergency response or fall detection systems, low anomaly detection latency <sup>2</sup> is vital for triggering actionable alerts. Figure 1(b) illustrates two detection curves achieving identical AUC/AP, but the first curve exhibits an earlier detection compared to the second. Although there are metrics that address detection latency in time series anomaly detection [21, 22] and continual VAD [23], they assume anomalies as isolated points rather than temporal events, rendering them inapplicable to generic VAD evaluation.

For benchmarking data, current large-scale datasets primarily collect videos from the internet or movies with various scenes. As exemplified in Figure 1(c), a typical limitation arises when a trained model is tested on scenes that are different from the training data. These test data are relatively easy for the model to detect and cannot tell whether the model is overfitted to the scene (e.g., taking a cramped grocery as an anomaly). The ideal test data should comprise videos of the same scene with different events (e.g., shopping in a cramped store peacefully). Though some datasets [24–28] collected by manual recording or 3D animations contain different behaviors in the same scene, they either lack severe anomalies (e.g., explosions), exhibit domain gaps from real-world data, or suffer from the limited scale of dataset samples.

In this paper, we focus on better evaluation methods for VAD algorithms. **First**, we systematically analyze the three aforementioned limitations on three large-scale VAD datasets (UCF-Crime [13], XD-Violence [15], MSAD [14]) through multi-round re-annotation (i.e., each round is labeled by different annotators) and exploratory experiments. **Second**, we propose averaged AUC/AP metrics to mitigate annotation bias and a novel Latency-aware Average Precision (LaAP) metric to evaluate the latency of VAD algorithms. The averaged AUC/AP calculate the AUC/AP of each round of annotation and take the average. The LaAP replaces AP's Precision-Recall curve with a Precision-LaRecall curve, where LaRecall rewards earlier detections of anomalies through a time-decaying weighting mechanism. This metric also maintains the capability to evaluate model performance across varying thresholds. **Third**, we construct two synthetic benchmarks (UCF-HN & MSAD-HN) via image-to-video diffusion models [29, 30] to evaluate overfitting in VAD algorithms. UCF-HN and MSAD-HN comprise normal videos generated from keyframes of abnormal scenes in UCF-Crime and MSAD training sets, where high false alarm rates (FAR) on these data reflect overfitting.

Extensive experiments validate the reliability of the proposed metrics and the realism of the proposed synthetic benchmarks. We report performance comparisons on ten state-of-the-art (SOTA) open-source VAD models [3–5, 7–10, 31–33] with our new evaluation methods. The comparisons reveal two critical findings: 1) Some methods demonstrating strong performance under conventional metrics

<sup>2</sup>The *latency* in this paper denotes how rapidly scores rise after an anomaly occurs rather than computational throughput.

exhibit degraded performance on our proposed metrics, suggesting overfitting to annotation bias or having large latency; 2) Existing methods have high false alarm rates on the new benchmarks, suggesting vulnerable generalization. Our contributions are summarized as follows:

1. We propose the annotation-averaged AUC/AP metrics and the LaAP metric, which mitigate annotation bias and reward early anomaly detection.
2. We construct the UCF-HN and MSAD-HN benchmarks with hard normal videos generated via diffusion models to evaluate scene overfitting in VAD methods.
3. We report results for SOTA VAD methods using our proposed evaluation framework and provide new perspectives into model behaviors.

## 2 Related Works

### 2.1 Video Anomaly Detection Metrics

The majority of existing works employ AUC and AP as evaluation metrics. Here, AUC represents the area under the TPR (True Positive Rate)-FPR (False Positive Rate) curve, while AP denotes the area under the Precision-Recall curve. Compared to Accuracy and F1-score, both metrics comprehensively evaluate the performance under varying decision thresholds, with AUC being insensitive to class imbalance [34] and AP demonstrating better capability for positive instances [15]. Despite criticisms of these metrics [34, 35], they remain widely adopted in medical diagnosis [36], object detection [37], and recommendation systems [38]. In video anomaly detection, anomalies typically manifest as continuous multi-frame events, and early detection of such anomalies is often prioritized in practical applications. However, both AUC and AP treat predictions as independent instances, thereby neglecting the event-based nature of anomalies and exhibiting insensitivity to detection latency. While the NAB metric [22] in time-series anomaly detection and the APD metric [23] in continual learning VAD incorporate prediction latency, they model anomalies as discrete points and measure delays within a fixed time window, which overlook variations in duration of abnormal events, rendering them suboptimal for VAD evaluation. There are also metrics concerning spatiotemporal localization (e.g., TBDC [39], STAUC [40]) or multi-class classification (e.g., mAP@IoU [10]), but we focus on temporal detection performance in VAD. Moreover, existing metrics only utilize single-round annotation per test video, potentially introducing annotator bias as discussed in [18, 41, 42].

Inspired by them, we propose the Latency-aware Average Precision (LaAP), which rewards early anomaly detection through an adaptive time window and nonlinear score functions, offering a novel perspective for VAD evaluation. We also conduct independent re-annotations for three large-scale datasets, where the averaging metric helps mitigate individual annotator bias.

### 2.2 Video Anomaly Detection Benchmarks

Current VAD benchmarks predominantly adopt in-domain evaluation, with few works [41, 42, 44–46] employing cross-domain approaches. The in-domain protocol evaluates models on test sets corresponding to their training data, whereas the cross-domain protocol evaluates generalization capability using test sets from different datasets. Table 1 compares existing VAD datasets. [24–26, 28, 43] manually record videos with actors performing abnormal events, but these datasets suffer from limited scale and lack severe anomaly events (e.g., explosions). [27] utilizes synthetic 3D animations to generate videos, but it introduces significant discrepancies from real-world data. [13–15] collect videos from the web and movies, greatly expanding anomaly categories and scale. However, unlike manually recorded datasets, they fail to provide both normal and abnormal videos of the same scene, making it challenging to determine whether the model has overfitted to scenes rather than the true anomaly patterns. For instance, a dataset might contain an abnormal video showing a van exploding at a gas station, but lack normal videos where the same van

Table 1: Comparisons of VAD datasets. *Intra-Scene Pos&Neg* denotes the inclusion of both normal and abnormal videos of the same scene.

Dataset	Source	# videos	Intra-Scene Pos&Neg
Subway [25]	recorded	2	✓
UCSD Ped [43]	recorded	98	✓
Avenue [24]	recorded	35	✓
ShanghaiTech [28]	recorded	437	✓
NWPU Campus [26]	recorded	547	✓
UBNormal [27]	synthesized	543	✓
UCF-Crime [13]	web	1900	✗
XD-Violence [15]	web, movie	4754	✗
MSAD [14]	web	720	✗

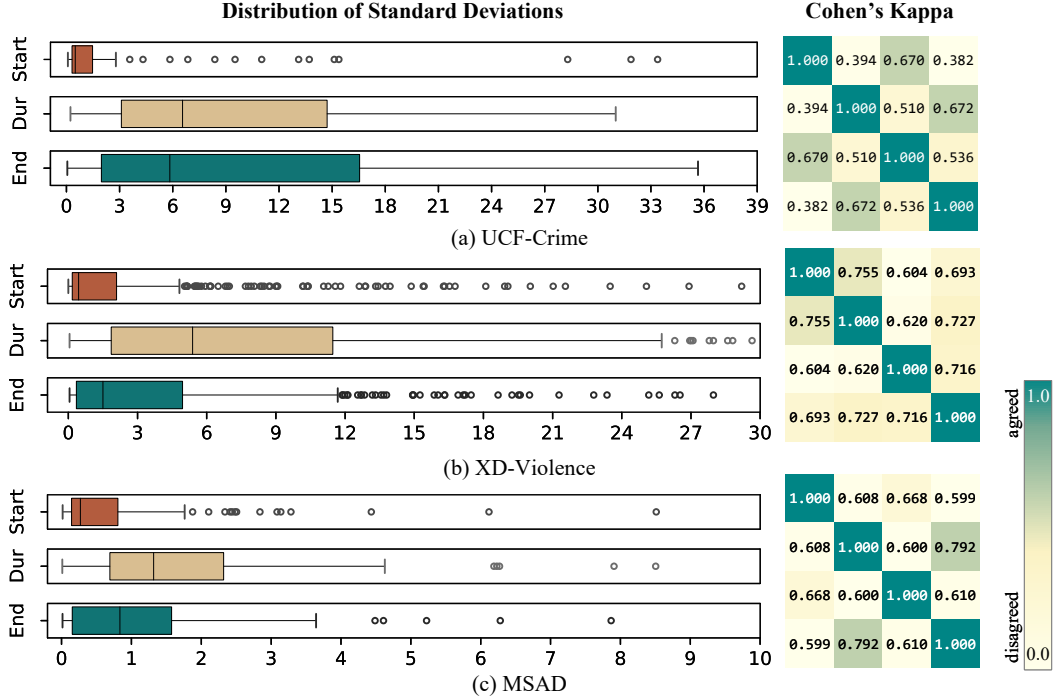


Figure 2: **Left:** The distribution of standard deviations for start time, duration, and end time (in seconds) across different annotations in three datasets. **Right:** The pair-wise Cohen’s Kappa between annotators.

refuels and departs safely at the same gas station. An overfitting model might consider gas stations or vans as anomalies, yet both in-domain and cross-domain benchmarks cannot evaluate that.

To address these issues, we construct UCF-HN and MSAD-HN, generated via image-to-video diffusion models [29, 30], which synthesize normal behaviors under identical scenes to evaluate overfitting.

### 3 Analysis of Current Metrics and Benchmarks

#### 3.1 Bias Prevails in Annotations

The validity of evaluation metrics depends on the precision of annotations. In this section, we systematically analyze annotation discrepancies by re-annotating three large-scale datasets. Specifically, we select UCF-Crime [13], XD-Violence [15], and MSAD [14] datasets, among which MSAD represents a newer dataset featuring broader anomaly categories and higher video resolutions. Dataset details are provided in the supplementary Section C.

We re-annotate frame-level temporal boundaries for all abnormal videos in the test sets of these three datasets, strictly adhering to the original papers’ criteria. Each annotation round is assigned to a different annotator for independent labeling. This process yields four independent annotation rounds per dataset, including their vanilla annotations. Notably, for UCF-Crime, one round is from [18]. On UCF-Crime, we find that some abnormal videos have category ambiguity. Consequently, we perform additional categorical annotation on all abnormal videos of UCF-Crime.

We quantify the overall frame-level annotation consistency across three re-annotated datasets using Cohen’s Kappa [47] and Fleiss’ Kappa [48] in Figure 2 and Table 2. Both metrics range in  $[-1, 1]$  where values approaching 1 indicate perfect agreement. The results reveal that the lowest inter-annotator Cohen’s Kappa is 0.382, with overall Fleiss’ Kappa ranging from 0.51 to 0.68, indicating

Table 2: The overall Fleiss’ Kappa and the median of standard deviations for start time, duration, and end time (in seconds).

	UCF	XD	MSAD
Fleiss’ Kappa $\uparrow$	0.51	0.68	0.64
median of start std $\downarrow$	0.50	0.44	0.27
median of duration std $\downarrow$	6.56	5.39	1.32
median of end std $\downarrow$	5.84	1.50	0.83

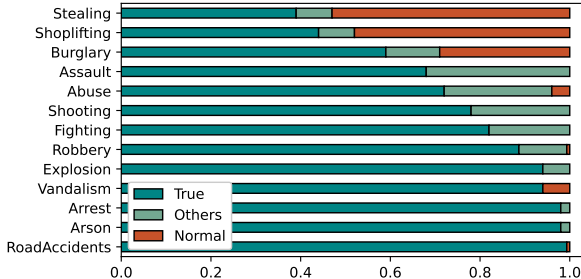


Figure 3: Visualization of discrepancies in UCF-Crime [13]. **True** indicates agreement between annotations; **Others** denotes our annotation assigning the sample to another anomaly category; **Normal** denotes videos classified as normal.

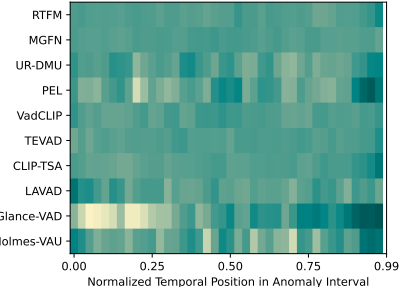


Figure 4: Heatmap of predicted anomaly positions of different models [3–5, 7–10, 31–33] in abnormal intervals. Brighter areas indicate higher density.

substantial annotation discrepancies. To identify the source of discrepancies, we analyze the distribution of standard deviations of start time, duration, and end time in Figure 2 and Table 2. Note that the start and end times correspond to the earliest and latest annotated abnormal frames in a video, and the duration refers to the total time of all annotated abnormal segments in a video. The results reveal that the deviations for the duration and end time are significantly higher than those for the start time, which indicates that annotators diverge in granularity (i.e., whether to label the most salient segments or more comprehensive events) and determination of ending (i.e., whether to label the aftermath).

Figure 3 visualizes the categorical discrepancies between the original annotation and ours in UCF-Crime. Videos originally labeled as *Stealing*, *Shoplifting*, and *Burglary* exhibit high rates of “misclassification” as *Normal* ( $\geq 30\%$ ). We attribute this to inherent dependence on contextual information beyond the video. For instance, it is challenging to distinguish between the staff member’s routine actions and a shoplifter’s behavior of taking away a t-shirt in surveillance footage without knowing who the staff member is. Such ambiguous instances introduce confounding signals during training. Visualization examples of annotation bias are given in Section C.3.

### 3.2 Existing Methods Differ in Latency

In practical applications, accurate and early anomaly detection is preferable under equivalent model capability. However, current metrics treat VAD task as a frame-independent binary classification task while neglecting positional information in predictions.

Figure 4 illustrates the distribution of prediction latency across multiple models. We select prediction scores within abnormal intervals, binarize them, obtain the positions of positive instances, and normalize them using the length of the abnormal interval. The results reveal that certain models (e.g., RTFM [3], CLIP-TSA [8]) exhibit relatively uniform predictions, while some (PEL [9], Glance-VAD [32]) achieve higher positive concentrations in earlier stages, indicating differences exist in models’ capability of predicting latency.

### 3.3 Current Benchmarks Struggle to Evaluate Scene Overfitting

Existing VAD models trained on web-sourced large-scale datasets [13–15] may risk overfitting to training scenes, yet current benchmarks cannot fully evaluate the overfitting, because they comprise scenes different from training data and fail to evaluate whether models retain performance on scenes that closely resemble training conditions. For instance, the production scenario may be a crowded grocery store with a checkout counter on the right, which is included in the training data, while existing test data only comprises videos of mobile phone stores and clothing retailers.

Therefore, we conduct a preliminary experiment by re-splitting the ShanghaiTech dataset [28] as shown in Table 3. ShanghaiTech is a manually recorded dataset with normal and abnormal

Table 3: Re-splitting strategy and performance of on the re-split ShanghaiTech.

Split	Re-split Scene Number		Performance(%)	
	Normal	Abnormal	AUC	FAR <sub>0.5</sub>
train set	01-06	07-10	-	-
easy test set	11,12,13	11,12,13	94.55	0.38
hard test set	07-10	01-06	16.35	44.10

videos across 13 scenes. We first construct a training set and an easy test set to simulate the case of web-sourced datasets like UCF-Crime, where each scene in the training set contains exclusively normal or exclusively abnormal videos, with test scenes being distinct from those in the training set. Subsequently, we construct a hard test set containing identical scenes to the training set but with reversed video normality in the same scenes. We train PEL [9] on the training set, evaluate on both test sets with the best checkpoint. As shown in Table 3, while the model demonstrates satisfactory performance on the easy test set, which simulates existing benchmarks, it significantly deteriorates on the hard test set, resulting in a sharp AUC drop to 16% with a high 44% FAR, indicating severe scene overfitting.

## 4 Proposed Metrics and Benchmarks

### 4.1 Annotation Averaged AUC and AP Metrics

To mitigate the impact of bias in single-round annotation, one straightforward solution is to standardize the annotation process, particularly regarding granularity and ending criteria. However, this is challenging given the complexity and diversity of anomalies. Alternative approaches include employing soft labels or aggregating via voting mechanisms, but they either fail to be compatible with the existing metrics or cause information loss. Consequently, we propose to calculate AUC/AP separately across annotations and use the averages as more reliable metrics, which avoids the aforementioned drawbacks. Formally,

$$\text{AUC}_{\text{avg}} = \sum_{r=0}^R \text{AUC}(\hat{\mathcal{Y}}, \mathcal{Y}_r)/R, \quad \text{AP}_{\text{avg}} = \sum_{r=0}^R \text{AP}(\hat{\mathcal{Y}}, \mathcal{Y}_r)/R, \quad (1)$$

where  $\hat{\mathcal{Y}}$  is the model predictions,  $\mathcal{Y}_r$  is the  $r$ -th round annotation, and  $R$  denotes the number of annotation rounds.

### 4.2 Latency-aware AP Metric

Motivated by the latency sensitivity of real-world anomaly detection systems, we introduce Latency-aware Average Precision (LaAP) - a novel evaluation metric that expands the standard AP metric through a time-decaying weighting mechanism, explicitly rewarding earlier predictions. Formally, LaAP is defined as the area under the Precision-LaRecall curve under all possible thresholds  $\tau$ :

$$\text{LaAP} = \int_0^1 \text{LaRecall}(\tau) dP(\tau), \quad (2)$$

where the LaRecall replaces Recall in AP and is the core component. As illustrated in Figure 5, the computation of LaRecall involves four steps:

(1) **Thresholding:** Convert predicted probabilities to binary labels given a threshold:

$$\bar{Y}^j = \{\bar{y}_i^j\}_{i=1}^{M_j}, \quad \bar{y}_i^j = \mathbb{1}(\hat{y}_i^j \geq \tau), \quad (3)$$

where  $\hat{y}$  denotes the model prediction scores, the superscript  $j$  denotes  $j$ -th video in the dataset, the subscript  $i$  denotes  $i$ -th frame in the video,  $M_j$  denotes number of frames in the  $j$ -th video, and  $\bar{Y}^j$  is the binary labels.

(2) **Sparse Sampling:** Sample multiple key detection frames from positive predictions, ensuring temporal spacing  $\phi$  between consecutive detections:

$$\mathcal{A}^j = \text{Sample}(\bar{Y}^j), \quad \mathcal{A}_{k+1}^j - \mathcal{A}_k^j > \phi, \quad (4)$$

where  $\mathcal{A}$  denotes the indices of sampled frames and the subscript denotes  $k$ -th sampled frame. The selection of multiple detections helps to reduce the influence of noise, and the spacing is set to avoid repeated scoring.

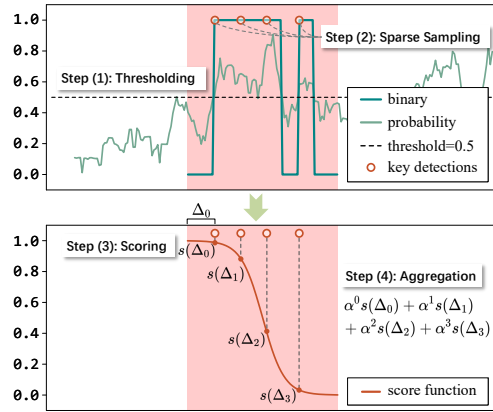


Figure 5: Visualization of the computational steps of LaRecall.

(3) **Scoring:** Apply a Sigmoid-like time-decaying scoring function to the sampled detections, which can give a score close to 1 during a short period after the anomaly occurs, followed by a smooth decrease to 0. This property aligns with the intuition of rewarding early detection. Formally,

$$s(\Delta_k^j) = 1 - \frac{1}{1 + \exp(-\beta(2\Delta_k^j - 1))}, \quad \Delta_k^j = \frac{\mathcal{A}_k^j - t_{\text{start}}}{t_{\text{end}} - t_{\text{start}}}, \quad (5)$$

where  $t_{\text{start}}, t_{\text{end}}$  denote the indices of the start frame and the end frame, respectively, and  $\beta$  controls the curve shape.

(4) **Aggregation:** Compute video-level LaRecall through exponentially decaying weighted function  $w(k) = \alpha^k$ , and then average across all abnormal videos. Specifically, if a video yields no positives under a given detection threshold, the corresponding LaRecall score is set to zero.

$$\text{LaRecall} = \sum_{j=0}^{N_a} \frac{\sum_{k=0}^{|\mathcal{A}^j|-1} w(k)s(\Delta_k^j)}{\sum_{k=0}^{|\mathcal{A}^j|-1} w(k)}, \quad (6)$$

where  $N_a$  is the number of abnormal events in the dataset,  $|\mathcal{A}^j|$  denotes the number of sampled frames,  $\Delta_k^j$  denotes the normed position of the  $k$ -th detection in the  $j$ -th video, and  $\alpha$  are parameters controlling decaying degree.

In practice, LaAP assumes that only one abnormal event exists in a video due to the sparsity of anomalies. In existing datasets, almost all data satisfy this assumption except for the XD-Violence dataset, which has many heavily edited videos and contains multiple logically unrelated events within a single video. Consequently, we do not compute the LaAP metric on the XD-Violence dataset. For multi-round annotations, we select the median of the first abnormal frames and the latest abnormal frames across different annotations as the starting and ending times. This also mitigates the single annotation bias issue discussed in Section 3.1. Empirically, we set the parameter of LaAP as follows:  $\alpha = 2, \beta = 7, \phi = 16$ , where  $\alpha$  halves the weight of the next point,  $\beta$  builds a scoring function that is close to 1 or 0 at endpoints, and  $\phi$  ensures that the score is only calculated once in a short period.

### 4.3 Video-Diffusion-Generated Hard Normal Benchmarks

Having observed the severe overfitting in the re-split ShanghaiTech dataset, we raise the question: *Does the scene overfitting persist when training data contains more scenes?* However, validation becomes extremely challenging due to the inability to acquire the same-scene data in the real world. Therefore, leveraging advancements in AIGC technologies, we synthesize such data using video diffusion models [29, 30], which form two new hard normal benchmarks: UCF-HN and MSAD-HN.

Specifically, we first manually select scene keyframes from **abnormal** videos in the UCF-Crime and MSAD training sets. We prioritize frames with minimal subject interference, absence of motion blur, and high visual quality, which is better for diffusion models to generate high-quality videos. Only one keyframe is selected per video. Due to computational efficiency constraints, we sample a subset of videos for generation. Then, we use image-to-video diffusion models with instance-specific manual prompts to generate **normal** videos preserving identical scenes. Finally, we check all generated videos and re-generate videos that exhibit low quality or artifacts. For some videos, multiple normal samples are synthesized, yielding 100 hard normal samples for UCF-HN and 67 hard normal samples for MSAD-HN, which last from 10 to 16 seconds. Due to the complexity of abnormal actions and inability of generating multi-shot videos, we only generate normal videos and exclude XD-Violence. We provide both quantitative and qualitative validation of the realism of generated videos in the following experiments.

To perform benchmarking, the model should be trained on UCF-Crime or MSAD, and then be tested on the corresponding hard normal set. Since all test videos are normal, the false alarm rate (FAR) reflects the degree of overfitting. More details and visualizations of the benchmarks are in the supplementary Section F.

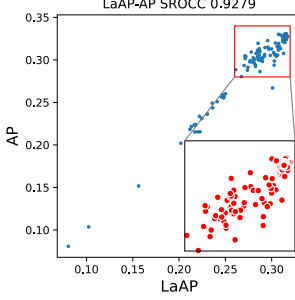


Figure 6: Correlation analysis between LaAP and AP.

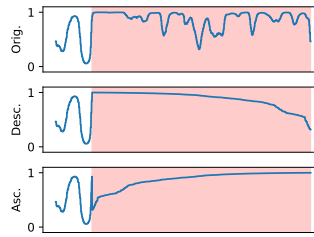
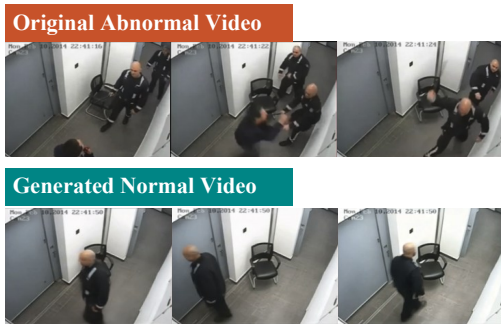


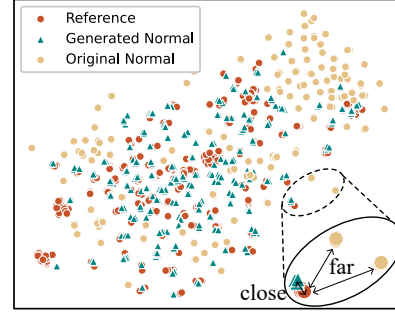
Figure 7: Visualization of different score modification methods.

Table 4: Comparisons between AUC, AP, and LaAP under different score modification methods. Our proposed LaAP is able to effectively reward earlier detections.

Model	Modification	AUC	AP	LaAP
VadCLIP	Desc.	0.900	0.486	0.783
	Ori.	0.900	0.486	0.740
	Asc.	0.900	0.486	0.675
PEL	Desc.	0.886	0.439	0.744
	Ori.	0.886	0.439	0.727
	Asc.	0.886	0.439	0.645



(a) Comparison between a reference video and the corresponding generated video in UCF-HN



(b) T-SNE Visualization of reference abnormal videos, generated normal videos, and original normal videos

Figure 8: Visualizations of our proposed synthetic benchmarks.

## 5 Experiments

### 5.1 Baselines

We reproduced 10 SOTA VAD methods spanning four methodological groups: 1) Traditional methods (RTFM [3], MGFN [4], UR-DMU [5]); 2) Text-enhanced methods (PEL [9], VadCLIP [10], TEVAD [7], CLIP-TSA [8]); 3) Zero-shot methods (LAVAD [31]); 4) Extra supervision methods (GlanceVAD [32], HolmesVAU [33]). With priority given to officially released weights, we retrained unavailable models using their original implementations. Details of baselines are provided in the supplementary Section D.

### 5.2 Reliability of LaAP

In Figure 6, we plot the AP and LaAP values and calculate the Spearman’s Rank-Order Correlation Coefficient (SROCC) during the training of VadCLIP, which shows strong correlation between LaAP and AP. To investigate the advantages of LaAP, we conduct a comparative analysis by modifying predicted scores from VadCLIP [10] and PEL [9] on UCF-Crime [13]. As illustrated in Figure 7, we simulate early/late detection through temporal reordering of anomaly scores within abnormal segments while preserving original score magnitudes. The *Desc.* makes the detection earlier by sorting scores in descending order, while *Asc.* achieves the opposite effect through ascending order. Table 4 demonstrates LaAP’s latency awareness: While AUC/AP remain invariant, our LaAP effectively rewards earlier detections through its temporal weighting mechanism.

### 5.3 Realism of UCF-HN and MSAD-HN

To validate the realism of our synthetic data, Figure 8(a) visually compares an original anomaly video (showing “Abuse”) with its generated normal counterpart, where violent actions are replaced by natural walking while maintaining perfect background coherence. Figure 8(b) further analyzes

Table 5: Comparisons between UBNormal, UCF-HN and MSAD-HN with FID [49] and FVD [50] metrics.

Datasets	FID	FVD
UBNormal [27]	202.6	698.0
UCF-HN	149.5	530.2
MSAD-HN	140.4	461.0

Table 6: Comparisons between various state-of-the-art VAD models with original AUC/AP (Orig.), our proposed averaged AUC/AP (Avg.), and our proposed LaAP metric. Note that the metrics on UCF-Crime exclude three categories as discussed in Section 3.1. The scores are colored according to the rank. \* denotes zero-shot methods. † denotes methods with extra supervision signals.

Model	UCF-Crime				XD-Violence				MSAD					
	AUC		AP		LaAP		AUC		AP		AUC			
	Orig.	Avg.	Orig.	Avg.	LaAP	Orig.	Avg.	Orig.	Avg.	Orig.	Avg.	Orig.	Avg.	LaAP
Random	0.499	0.500	0.075	0.135	0.129	0.500	0.500	0.231	0.259	0.497	0.498	0.228	0.213	0.267
RTFM [3]	0.835	0.859	0.239	0.388	0.480	-	-	-	-	0.868	0.867	0.662	0.645	0.713
MGFN [4]	0.820	0.863	0.216	0.384	0.761	-	-	-	-	0.850	0.846	0.633	0.607	0.664
UR-DMU [5]	0.887	0.876	0.275	0.442	0.693	0.940	0.941	0.817	0.841	0.878	0.869	0.697	0.663	0.729
PEL [9]	0.890	0.886	0.305	0.439	0.727	0.949	0.945	0.855	0.861	0.873	0.869	0.676	0.659	0.729
VadCLIP [10]	0.889	0.900	0.254	0.486	0.740	0.947	0.952	0.845	0.870	0.878	0.865	0.597	0.541	0.665
TEVAD [7]	0.874	0.861	0.265	0.408	0.599	0.923	0.913	0.798	0.814	-	-	-	-	-
CLIP-TSA [8]	0.900	0.913	0.272	0.470	0.695	0.932	0.933	0.772	0.807	-	-	-	-	-
LAVAD* [31]	0.856	0.842	0.336	0.446	0.592	0.854	0.859	0.620	0.687	-	-	-	-	-
GlanceVAD <sup>†</sup> [32]	0.937	0.906	0.484	0.558	0.818	0.959	0.955	0.892	0.891	-	-	-	-	-
HolmesVAU <sup>†</sup> [33]	0.893	0.912	0.321	0.547	0.800	-	-	-	-	-	-	-	-	-

Table 7: Performance comparison of SOTA VAD methods on UCF-Crime/MSAD and our proposed hard-normal variants (UCF-HN/MSAD-HN) using  $\text{FAR}_\tau$  metric, where  $\tau$  is the threshold. The scores are colored according to the value.

Model	Supervision	Original UCF Test				UCF-HN		Original MSAD Test				MSAD-HN	
		FAR <sub>0.5</sub>	FAR <sub>0.8</sub>										
CLIP-TSA [8]	Weak	0.055	0.034	1.000	1.000	-	-	-	-	-	-	-	-
RTFM [3]	Weak	0.129	0.049	0.823	0.625	0.050	0.020	0.236	0.046	0.145	0.063	0.866	0.604
PEL [9]	Weak	0.005	0.001	0.562	0.393	0.001	0.000	0.866	0.604	0.136	0.064	0.700	0.676
VadCLIP [10]	Weak	0.024	0.008	0.442	0.292	0.077	0.050	1.000	1.000	-	-	-	-
MGFN [4]	Weak	0.033	0.012	0.300	0.294	0.565	0.382	-	-	-	-	-	-
UR-DMU [5]	Weak	0.011	0.002	0.180	0.171	0.136	0.064	0.700	0.676	-	-	-	-
UR-DMU [32]	Glance	0.016	0.003	0.219	0.129	-	-	-	-	-	-	-	-
UR-DMU [33]	Full	0.005	0.000	0.136	0.000	-	-	-	-	-	-	-	-

the feature-space relationships: Our hard negative samples demonstrate closer proximity to abnormal videos than original normal videos. We further compute Fréchet Inception Distance (FID) [49] and Fréchet Video Distance (FVD) [50] between UBNormal [27] and our method on real-world surveillance videos, which comprise videos of original test sets in UCF-Crime and MSAD. As in Table 5, significantly lower values demonstrate the superior realism of our benchmarks.

#### 5.4 Benchmarking Existing Methods

We report the performance of SOTA VAD methods with our proposed averaged AUC/AP, LaAP and hard normal benchmarks in Tables 6,7. From Table 6, we observe that using averaged instead of original AUC/AP values significantly impacts method rankings, demonstrating that metric reliability is affected by annotator disagreements. This effect is most pronounced on UCF-Crime, while being relatively minor on XD-Violence and MSAD, which aligns with our observations of annotation discrepancy discussed in Section 3.1. Furthermore, comparative analysis of LaAP metrics reveals that models with comparable AUC/AP may exhibit substantial differences in LaAP. For instance, on UCF-Crime, MGFN underperforms other methods in both AUC and AP metrics but achieves the highest LaAP among weakly-supervised approaches. Similarly on MSAD, UR-DMU and VadCLIP demonstrate identical AUC performance yet exhibit significant LaAP discrepancy. Experiments also confirm that methods incorporating additional supervisory signals achieve consistent improvements across all metrics.

From Table 7, while most methods maintain low FAR ( $\leq 10\%$ ) on the original test set, they suffer dramatic performance degradation on our proposed hard normal benchmarks. We observe a 42% average increase at 0.5 threshold, and 36% at 0.8 threshold, with some methods exceeding 70% FAR. This reveals severe scene overfitting in existing approaches. Comparative studies of supervision strategies using the same UR-DMU backbone reveal that clearer supervisory signals can mitigate overfitting risks. Although current anomaly videos in the training sets contain both normal and abnormal intervals, video-level weak supervision struggles to guide models in learning true anomaly patterns.

## 6 Conclusion

In this paper, we reveal critical limitations in current metrics and benchmarks of VAD through systematic analysis. To address these limitations, we propose new metrics for reliable and latency-sensitive evaluation (i.e., averaged AUC/AP and LaAP). We also construct new benchmarks to evaluate the model generalizability (i.e., UCF-HN and MSAD-HN). We benchmark various SOTA VAD methods according to our new evaluation methods, providing novel perspectives on evaluating VAD algorithms.

## References

- [1] S. Chandrakala, K. Deepak, and G. Revathy. Anomaly detection in surveillance videos: a thematic taxonomy of deep models, review and performance analysis. *Artif. Intell. Rev.*, 56(4):3319–3368, 2023.
- [2] Peng Wu, Chengyu Pan, Yuting Yan, Guansong Pang, Peng Wang, and Yanning Zhang. Deep learning for video anomaly detection: A review. *arxiv preprint*, abs/2409.05383, 2024.
- [3] Yu Tian, Guansong Pang, Yuanhong Chen, Rajvinder Singh, Johan W. Verjans, and Gustavo Carneiro. Weakly-supervised video anomaly detection with robust temporal feature magnitude learning. In *ICCV*, pages 4955–4966. IEEE, 2021.
- [4] Yingxian Chen, Zhengzhe Liu, Baocheng Zhang, Wilton W. T. Fok, Xiaojuan Qi, and Yik-Chung Wu. MGPN: magnitude-contrastive glance-and-focus network for weakly-supervised video anomaly detection. In Brian Williams, Yiling Chen, and Jennifer Neville, editors, *AAAI*, pages 387–395. AAAI Press, 2023.
- [5] Hang Zhou, Junqing Yu, and Wei Yang. Dual memory units with uncertainty regulation for weakly supervised video anomaly detection. In Brian Williams, Yiling Chen, and Jennifer Neville, editors, *AAAI*, pages 3769–3777. AAAI Press, 2023.
- [6] Hui Lv, Zhongqi Yue, Qianru Sun, Bin Luo, Zhen Cui, and Hanwang Zhang. Unbiased multiple instance learning for weakly supervised video anomaly detection. In *CVPR*, pages 8022–8031. IEEE, 2023.
- [7] Weiling Chen, Keng Teck Ma, Zi Jian Yew, Minhoe Hur, and David Aik-Aun Khoo. TEVAD: improved video anomaly detection with captions. In *CVPRW*, pages 5549–5559, Vancouver, CA, 2023. IEEE.
- [8] Hyekang Kevin Joo, Khoa Vo, Kashu Yamazaki, and Ngan Le. CLIP-TSA: clip-assisted temporal self-attention for weakly-supervised video anomaly detection. In *ICIP*, pages 3230–3234, Kuala Lumpur, Malaysia, 2023. IEEE.
- [9] Yujiang Pu, Xiaoyu Wu, Lulu Yang, and Shengjin Wang. Learning prompt-enhanced context features for weakly-supervised video anomaly detection. *TIP*, 33:4923–4936, 2024.
- [10] Peng Wu, Xuerong Zhou, Guansong Pang, Lingru Zhou, Qingsen Yan, Peng Wang, and Yanning Zhang. Vadclip: Adapting vision-language models for weakly supervised video anomaly detection. In Michael J. Wooldridge, Jennifer G. Dy, and Sriraam Natarajan, editors, *AAAI*, pages 6074–6082, Vancouver, Canada, 2024. AAAI Press.
- [11] Zhiwei Yang, Jing Liu, and Peng Wu. Text prompt with normality guidance for weakly supervised video anomaly detection. In *CVPR*, pages 18899–18908, Seattle, USA, 2024. IEEE.
- [12] Seongheon Park, Hanjae Kim, Minsu Kim, Dahye Kim, and Kwanghoon Sohn. Normality guided multiple instance learning for weakly supervised video anomaly detection. In *WACV*, pages 2664–2673. IEEE, 2023.
- [13] Waqas Sultani, Chen Chen, and Mubarak Shah. Real-world anomaly detection in surveillance videos. In *CVPR*, pages 6479–6488. Computer Vision Foundation, 2018.
- [14] Liyun Zhu, Lei Wang, Arjun Raj, Tom Gedeon, and Chen Chen. Advancing video anomaly detection: A concise review and a new dataset. In *NeurIPS*, volume 37, pages 89943–89977. Curran Associates, Inc., 2024.
- [15] Peng Wu, Jing Liu, Yujia Shi, Yujia Sun, Fangtao Shao, Zhaoyang Wu, and Zhiwei Yang. Not only look, but also listen: Learning multimodal violence detection under weak supervision. In *ECCV*, volume 12375 of *Lecture Notes in Computer Science*, pages 322–339. Springer, 2020.
- [16] Xiaohan Lan, Yitian Yuan, Xin Wang, Long Chen, Zhi Wang, Lin Ma, and Wenwu Zhu. A closer look at debiased temporal sentence grounding in videos: Dataset, metric, and approach. *ACM Trans. Multim. Comput. Commun. Appl.*, 19(6):218:1–218:23, 2023.

[17] Mayu Otani, Yuta Nakashima, Esa Rahtu, and Janne Heikkilä. Uncovering hidden challenges in query-based video moment retrieval. In *BMVC*. BMVA Press, 2020.

[18] Yashika Jain, Ali Dabouei, and Min Xu. Cross-domain learning for video anomaly detection with limited supervision. In *ECCV*, volume 15088 of *Lecture Notes in Computer Science*, pages 468–484. Springer, 2024.

[19] Hamza Karim, Keval Doshi, and Yasin Yilmaz. Real-time weakly supervised video anomaly detection. In *WACV*, pages 6834–6842. IEEE, 2024.

[20] Tongtong Yuan, Xuange Zhang, Kun Liu, Bo Liu, Chen Chen, Jian Jin, and Zhenzhen Jiao. Towards surveillance video-and-language understanding: New dataset, baselines, and challenges. In *CVPR*, pages 22052–22061. IEEE, 2024.

[21] Zahra Zamanzadeh Darban, Geoffrey I. Webb, Shirui Pan, Charu Aggarwal, and Mahsa Salehi. Deep learning for time series anomaly detection: A survey. *ACM Comput. Surv.*, 57(1):15:1–15:42, 2025.

[22] Subutai Ahmad, Alexander Lavin, Scott Purdy, and Zuha Agha. Unsupervised real-time anomaly detection for streaming data. *Neurocomputing*, 262:134–147, 2017.

[23] Keval Doshi and Yasin Yilmaz. Rethinking video anomaly detection - A continual learning approach. In *WACV*, pages 3036–3045, Waikoloa, USA, 2022. IEEE.

[24] Cewu Lu, Jianping Shi, and Jiaya Jia. Abnormal event detection at 150 FPS in MATLAB. In *ICCV*, pages 2720–2727. IEEE Computer Society, 2013.

[25] Amit Adam, Ehud Rivlin, Ilan Shimshoni, and David Reinitz. Robust real-time unusual event detection using multiple fixed-location monitors. *IEEE Trans. Pattern Anal. Mach. Intell.*, 30(3):555–560, 2008.

[26] Congqi Cao, Yue Lu, Peng Wang, and Yanning Zhang. A new comprehensive benchmark for semi-supervised video anomaly detection and anticipation. In *CVPR*, pages 20392–20401, Vancouver, Canada, 2023. IEEE.

[27] Andra Acsintoae, Andrei Florescu, Mariana-Iuliana Georgescu, Tudor Mare, Paul Sumedrea, Radu Tudor Ionescu, Fahad Shahbaz Khan, and Mubarak Shah. Ubnormal: New benchmark for supervised open-set video anomaly detection. In *CVPR*, pages 20111–20121, New Orleans, USA, 2022. IEEE.

[28] Jia-Xing Zhong, Nannan Li, Weijie Kong, Shan Liu, Thomas H. Li, and Ge Li. Graph convolutional label noise cleaner: Train a plug-and-play action classifier for anomaly detection. In *CVPR*, pages 1237–1246, Long Beach, USA, 2019. Computer Vision Foundation / IEEE.

[29] Fan Bao, Chendong Xiang, Gang Yue, Guande He, Hongzhou Zhu, Kaiwen Zheng, Min Zhao, Shilong Liu, Yaole Wang, and Jun Zhu. Vidu: a highly consistent, dynamic and skilled text-to-video generator with diffusion models. *arxiv preprint*, abs/2405.04233, 2024.

[30] Ang Wang, Baole Ai, Bin Wen, Chaojie Mao, Chen-Wei Xie, Di Chen, Feiwu Yu, Haiming Zhao, Jianxiao Yang, Jianyu Zeng, et al. Wan: Open and advanced large-scale video generative models. *arxiv preprint*, abs/2503.20314, 2025.

[31] Luca Zanella, Willi Menapace, Massimiliano Mancini, Yiming Wang, and Elisa Ricci. Harnessing large language models for training-free video anomaly detection. In *CVPR*, pages 18527–18536. IEEE, 2024.

[32] Huixin Zhang, Xiang Wang, Xiaohao Xu, Xiaonan Huang, Chuchu Han, Yuehuan Wang, Changxin Gao, Shanjun Zhang, and Nong Sang. Glancevad: Exploring glance supervision for label-efficient video anomaly detection. *arxiv preprint*, abs/2403.06154, 2024.

[33] Huixin Zhang, Xiaohao Xu, Xiang Wang, Jialong Zuo, Xiaonan Huang, Changxin Gao, Shanjun Zhang, Li Yu, and Nong Sang. Holmes-vau: Towards long-term video anomaly understanding at any granularity. *arxiv preprint*, abs/2412.06171, 2024.

[34] Davide Chicco and Giuseppe Jurman. The matthews correlation coefficient (MCC) should replace the ROC AUC as the standard metric for assessing binary classification. *BioData Min.*, 16(1), 2023.

[35] Jorge M Lobo, Alberto Jiménez-Valverde, and Raimundo Real. Auc: a misleading measure of the performance of predictive distribution models. *Global ecology and Biogeography*, 17(2):145–151, 2008.

[36] Mark H Zweig and Gregory Campbell. Receiver-operating characteristic (roc) plots: a fundamental evaluation tool in clinical medicine. *Clinical chemistry*, 39(4):561–577, 1993.

[37] Joseph Redmon, Santosh Kumar Divvala, Ross B. Girshick, and Ali Farhadi. You only look once: Unified, real-time object detection. In *CVPR*, pages 779–788. IEEE Computer Society, 2016.

[38] Steffen Rendle, Christoph Freudenthaler, Zeno Gantner, and Lars Schmidt-Thieme. BPR: bayesian personalized ranking from implicit feedback. In Jeff A. Bilmes and Andrew Y. Ng, editors, *UAI*, pages 452–461. AUAI Press, 2009.

[39] Bharathkumar Ramachandra and Michael J. Jones. Street scene: A new dataset and evaluation protocol for video anomaly detection. In *WACV*, pages 2558–2567. IEEE, 2020.

[40] Yu Yao, Xizi Wang, Mingze Xu, Zelin Pu, Yuchen Wang, Ella Atkins, and David Crandall. Dota: unsupervised detection of traffic anomaly in driving videos. *PAMI*, 2022.

[41] MyeongAh Cho, Taeoh Kim, Minho Shim, Dongyoong Wee, and Sangyoun Lee. Towards multi-domain learning for generalizable video anomaly detection. In Amir Globersons, Lester Mackey, Danielle Belgrave, Angela Fan, Ulrich Paquet, Jakub M. Tomczak, and Cheng Zhang, editors, *NeurIPS*, 2024.

[42] Zihao Liu, Xiaoyu Wu, Jianqin Wu, Xuxu Wang, and Linlin Yang. Language-guided open-world video anomaly detection. *arxiv preprint*, abs/2503.13160, 2025.

[43] Vijay Mahadevan, Weixin Li, Viral Bhalodia, and Nuno Vasconcelos. Anomaly detection in crowded scenes. In *CVPR*, pages 1975–1981. IEEE Computer Society, 2010.

[44] Peng Wu, Xuerong Zhou, Guansong Pang, Yujia Sun, Jing Liu, Peng Wang, and Yanning Zhang. Open-vocabulary video anomaly detection. In *CVPR*. IEEE, 2024.

[45] Fei Li, Wenxuan Liu, Jingjing Chen, Ruixu Zhang, Yuran Wang, Xian Zhong, and Zheng Wang. Anomize: Better open vocabulary video anomaly detection. *arxiv preprint*, abs/2503.18094, 2025.

[46] Chenting Xu, Ke Xu, Xinghao Jiang, and Tanfeng Sun. Plovad: Prompting vision-language models for open vocabulary video anomaly detection. *TCSVT*, 2025.

[47] Jacob Cohen. A coefficient of agreement for nominal scales. *Educational and psychological measurement*, 20(1):37–46, 1960.

[48] Joseph L Fleiss. Measuring nominal scale agreement among many raters. *Psychological bulletin*, 76(5):378, 1971.

[49] Martin Heusel, Hubert Ramsauer, Thomas Unterthiner, Bernhard Nessler, and Sepp Hochreiter. Gans trained by a two time-scale update rule converge to a local nash equilibrium. In *NeurIPS*, pages 6626–6637, 2017.

[50] Wilson Yan, Yunzhi Zhang, Pieter Abbeel, and Aravind Srinivas. Videogpt: Video generation using vq-vae and transformers. *arxiv preprint*, abs/arXiv:2104.10157, 2021.

[51] Jesse Davis and Mark Goadrich. The relationship between precision-recall and ROC curves. In *ICML*, volume 148 of *ACM International Conference Proceeding Series*, pages 233–240. ACM, 2006.

[52] Peter A. Flach and Meelis Kull. Precision-recall-gain curves: PR analysis done right. In *NeurIPS*, pages 838–846, 2015.

[53] Hoon Kim, Kangwook Lee, Gyeongjo Hwang, and Changho Suh. Crash to not crash: Learn to identify dangerous vehicles using a simulator. In *AAAI*, pages 978–985. AAAI Press, 2019.

[54] Marcella Astrid, Muhammad Zaigham Zaheer, Jae-Yeong Lee, and Seung-Ik Lee. Learning not to reconstruct anomalies. In *BMVC*, page 279. BMVA Press, 2021.

[55] Pradeep Narwade, Ryosuke Kawamura, Gaurav Gajbhiye, and Koichiro Niinuma. Synthetic video generation for weakly supervised cross-domain video anomaly detection. In *ICPR*, volume 15315 of *Lecture Notes in Computer Science*, pages 375–391. Springer, 2024.

[56] Tom Fawcett. An introduction to roc analysis. *Pattern recognition letters*, 27(8):861–874, 2006.

## A Limitation and Future Work

Although this study proposes two metrics for algorithm evaluation, their application remains confined to temporal localization and binary classification tasks. The current method does not extend to more granular evaluations such as spatial localization or multiclass classification, which could be developed in future research to establish a comprehensive evaluation system building upon the present work.

This research innovatively employs Artificial Intelligence-Generated Content (AIGC) technology to propose a method for evaluating model generalizability. However, our analysis reveals limitations in existing video generation methods, particularly in handling complex motion, small objects, temporal coherence, and prompt automation. Notwithstanding these challenges, we think that synthetically generated data exhibits substantial advantages over alternative data sources, as further elaborated in Section F.4. Subsequent studies could focus on developing scalable pipelines for producing high-quality synthetic video anomaly datasets.

## B Open-source

The annotations files, codes to reproduce main results, notebooks, codes for LaAP calculation, and raw videos of proposed benchmarks will be provided.

## C Details of Re-annotated Datasets

### C.1 Selected Datasets

**UCF-Crime** [13] is the first large-scale and most commonly used VAD dataset of weak supervision, which comprises 1,900 surveillance videos from the web, covering 13 crime-related categories. This dataset employed 10 human annotators and took several months, with each video being assigned to multiple annotators and the final results averaged. However, the authors did not explicitly elaborate on the specific annotation method or the approach of the averaging process.

**XD-Violence** [15] is another large-scale dataset with 4,754 videos with an audio channel, covering 6 violence-related categories. The videos in XD-Violence may be labeled with more than one anomaly class. Its videos mainly come from movies, news, and user-uploaded videos on the web, which inevitably involve a lot of editing. XD-Violence employs the same annotation protocol as UCF-Crime but still provides only a single round of annotation without specifying the averaging process.

**MSAD** [14] is a recently proposed multi-scenario dataset, which is collected across 14 distinct scenarios, covering 11 base categories. The anomaly categories comprise both human-related and non-human-related anomalies, including some less serious anomalies (e.g., people falling). Moreover, MSAD provides videos of higher resolution. The authors of MSAD have not mentioned the details of the annotation process.

### C.2 Details of Re-annotating

We re-annotated 2 rounds for UCF-Crime, 3 rounds for XD-Violence, and 3 rounds for MSAD. Each annotation round was implemented by a single annotator, with distinct annotators assigned to different rounds of annotation for the same dataset. During the annotation process, temporal segment annotations were applied to abnormal videos in the test set. Annotators were provided with the anomaly categories and definitions provided by each dataset, alongside explicit instructions that each video contained at least one abnormal segment. We used the VIDAT annotation tool<sup>3</sup>. Each video took an average of 1 minute to annotate.

Especially, we conducted multi-class re-annotation for all 950 abnormal videos in UCF-Crime, with annotators instructed to assign each video to one of 14 predefined categories (including the normal class). Notably, although only abnormal videos were subjected to this relabeling, annotators were not informed of this constraint. Furthermore, these annotators constitute a distinct group from those involved in the temporal segment annotation, thereby avoiding potential bias.

---

<sup>3</sup><https://github.com/anucvml/vidat>

### C.3 Visualizations of Annotation Discrepancies

Figure A shows several videos that our annotators considered normal. In the first example, an individual placing clothes into a bag and exiting the frame could represent shoplifting behavior or a legitimate transaction occurring outside the camera’s view. The second case depicts a group of individuals carrying objects from a residence, with no visual evidence of illegal entry. The third instance involves an individual taking boxes from a doorway, where the viewer doesn’t know if he is the owner. Although these videos do have corresponding criminal behaviors, it is impossible to judge according to the video without prior knowledge.

We also provide visualizations of multiple forms of annotation discrepancies across three datasets in Figure B, validating the motivation of using averaged AUC/AP.

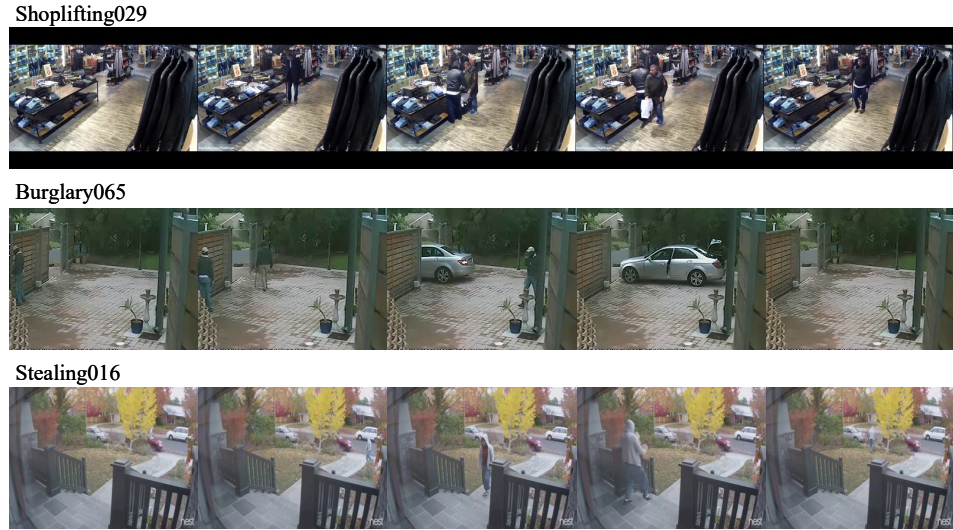
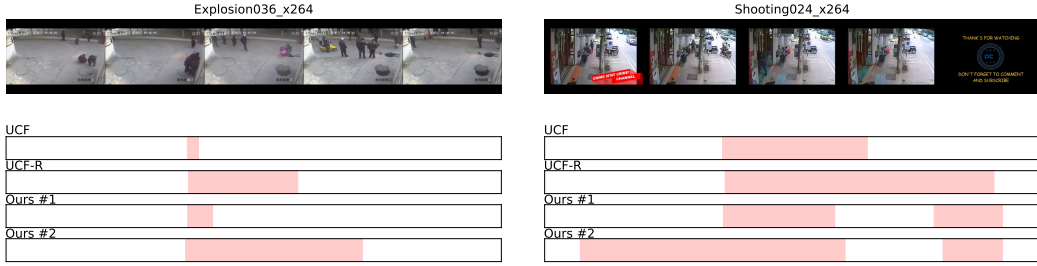


Figure A: Examples of multiclass annotation discrepancy in UCF-Crime. The abnormal events in these examples are hard to judge without further information.

## D Details of Baselines

This paper evaluates existing models on large-scale datasets using our proposed metrics and benchmarks. To facilitate comprehensive comparison, we implement 10 state-of-the-art VAD methods, which can be categorized into four groups based on their technical characteristics: (1) traditional methods employing the common weakly-supervised paradigm without external knowledge; (2) text-enhanced methods that integrate vision-language pre-trained models for performance enhancement; (3) zero-shot methods leveraging large models’ generalization capabilities to mitigate data bias and perform VAD task without tuning; and (4) methods utilizing additional supervision, which improve accuracy at the expense of requiring labor-intensive annotation. It is worth noting that UR-DMU [5], GlanceVAD [32], and HolmesVAU [33] use the same backbone, thus allowing us to compare the performance of different supervision paradigms more fairly. For the experimental setup, we retrain RTFM [3] and MGFN [4] on UCF-Crime, retrain UR-DMU [5], PEL [9], and VadCLIP [10] on MSAD, and directly employ official open-source weights for all other methods.

Moreover, we observe significant discrepancies in existing implementations of AP computation. Specifically, some approaches calculate the interpolated area under the precision-recall curve (e.g., using `sklearn.metrics.precision_recall_curve` combined with `sklearn.metrics.auc`), while others adopt non-interpolated computation (e.g., employing `sklearn.metrics.average_precision_score`). However, as demonstrated in [51, 52], interpolation may yield overly optimistic AP estimations. To ensure fair comparison, we consistently implement the non-interpolated AP metric throughout our experiments.



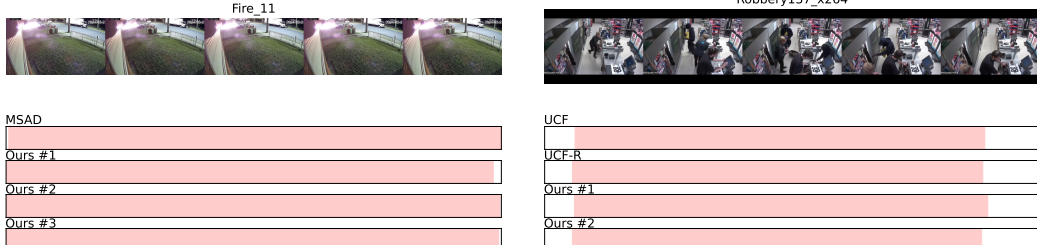
(a) The start time of the anomaly is more consistent than the end time.

(b) Different annotation granularity in a surveillance video.



(c) Different annotation granularity in a heavily edited video.

(d) Multiple independent abnormal events, where the start time of the anomaly is more consensual.



(e) Example of low discrepancy where the entire video is abnormal.

(f) Example of low discrepancy where the boundary of the abnormal event is clear.

Figure B: Examples of multiple forms of annotation discrepancies.

## E Further Evaluations

**Visualizations of predictions of models with different LaAP.** As illustrated in Figure Ca, PEL [9] demonstrates a significant improvement in prediction scores within the anomaly interval when compared to UR-DMU [5] and LAVAD [31]. Although LAVAD exhibits higher scores during the initial phase of the anomaly interval, UR-DMU manifests a lower false alarm rate in the normal part. From Figure Cb, we could find that methods with higher LaAP (UR-DMU, RTFM, PEL) give higher scores within the anomaly interval, and the others (VadCLIP, MGFN) either have higher scores on the normal part or lower scores on the abnormal part. These visualization examples further demonstrate the reliability of the proposed LaAP in evaluating detection latency.

**Comparisons between AP and LaAP.** In Figure D, we visualize curves for AP and LaAP on two datasets. We find a large difference in UCF-Crime and a smaller difference in MSAD, possibly caused by the shorter video length on MSAD. Additionally, the curves for both LaAP and AP exhibit similar properties. Specifically: (1) They invariably traverse the critical  $(0, 1)$  coordinate point; (2) They do not necessarily traverse the  $(1, 0)$  point; and (3) Both demonstrate non-monotonically decreasing characteristics.

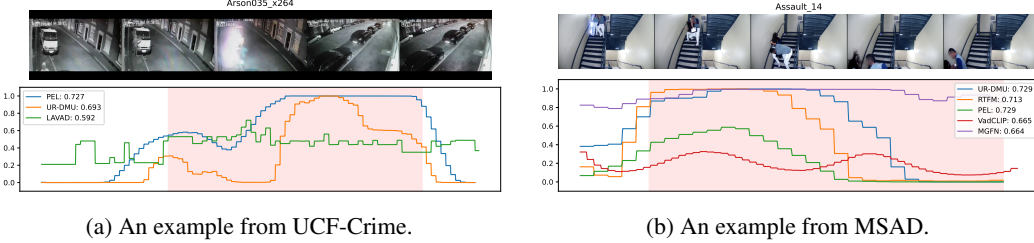


Figure C: Examples of predictions of models with different LaAP. The dataset level LaAP for each model is listed in the legend, and note that LaAP, like AUC/AP, cannot be analyzed at the instance level.

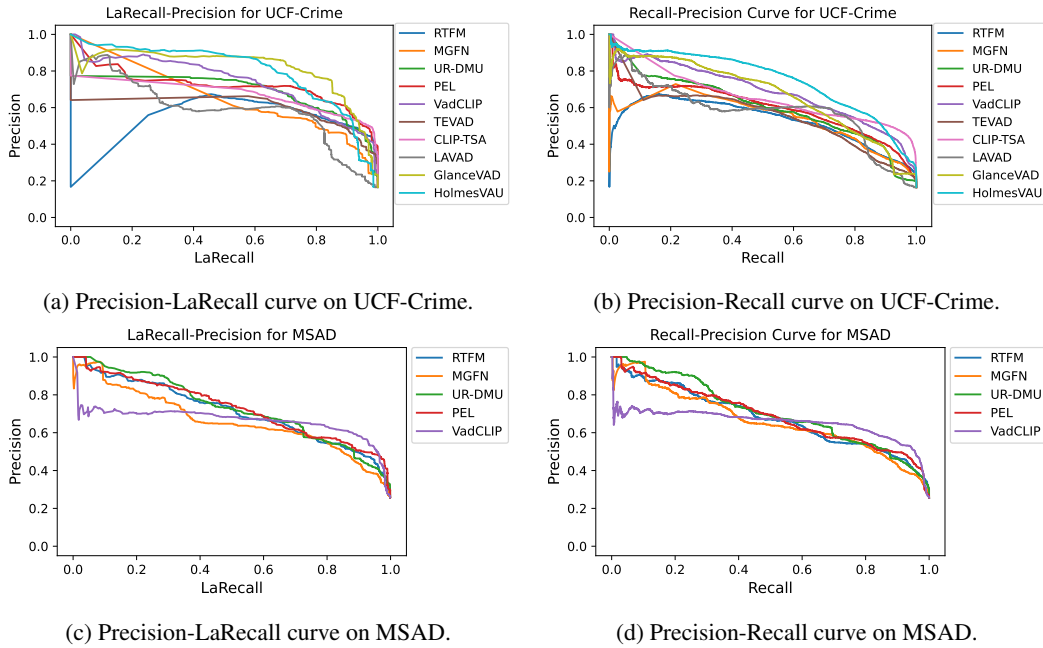
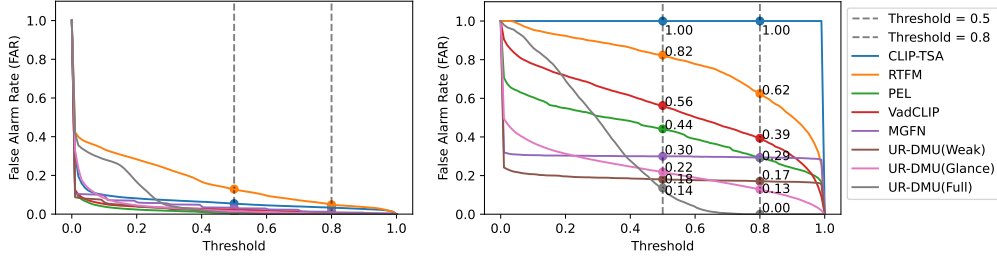
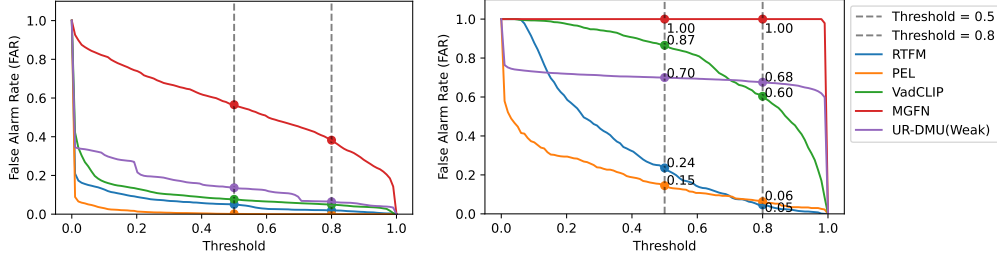


Figure D: Precision-LaRecall curve and Precision-Recall curve of existing models on UCF-Crime and MSAD.

**Visualizations of FAR under different thresholds.** Figure E visually presents the FAR curves of all methods discussed in the main text, with specific annotation of FAR scores at both a balanced threshold (0.5) and a conservative threshold (0.8). Comparative analysis between performance on the original test set and the hard normal test set reveals significant elevation among the curves. This empirical evidence demonstrates that models exhibit systematically higher FAR across varying thresholds in the hard normal test set, thereby confirming the efficacy of our proposed benchmarks in revealing model overfitting to backgrounds. In addition, we can find that some models have higher FAR than others under the balanced threshold, but lower under the conservative threshold. By analyzing the curve, we can choose a more appropriate model according to the actual needs. For example, the user may select the threshold according to the requirement of FAR (e.g.,  $\leq 0.1\%$ ), and calculate the LaRecall for model selection.



(a) FAR curves on UCF-Crime (left) and UCF-HN (right).



(b) FAR curves on MSAD (left) and MSAD-HN (right).

Figure E: FAR curves of different methods at different thresholds, on the left are the results on original datasets (UCF-Crime and MSAD), and on the right are the results on the proposed hard normal datasets (UCF-HN and MSAD-HN).

## F More Details of the Hard Normal Benchmarks

### F.1 Construction of UCF-HN and MSAD-HN.

The purpose of constructing UCF-HN and MSAD-HN is to evaluate the degree of model overfitting by generating normal videos with the same scene for abnormal videos. We construct UCF-HN and MSAD-HN in three steps as follows:

- **Select Keyframes.** To obtain high-quality images, we manually extracted key frames from anomaly videos in the training sets of UCF-Crime and MSAD. These keyframes met the following criteria: 1) No inclusion of abnormal events; 2) Absence of motion blur; 3) Minimal visible watermarks; 4) One keyframe per video.
- **Generate Videos.** For UCF-HN, we employed the image-to-video generation mode of Vidu 2.0 model from vidu platform<sup>4</sup> with 1088×800 resolution at 32 fps. For MSAD-HN, we utilized the wan2.1\_i2v\_480p\_14B model through ComfyUI<sup>5</sup> at 832×480 resolution with 16 fps. Each video was created by first generating a clip from the selected key frame, then producing an extended clip using the last frame of the first clip, followed by temporal concatenation. UCF-HN videos contain 15-second sequences while MSAD-HN videos comprise 10-second sequences. Manual prompt engineering ensured diverse event representations in generated videos. All key frames generated single videos except four key frames in UCF-HN, each producing five videos of different behaviors for granular analysis.
- **Recheck.** During this phase, we re-generate videos exhibiting suboptimal quality while discarding frames with persistent synthesis artifacts. All retained videos were subjected to manual quality inspection to verify visual fidelity. This process culminated in the creation of two benchmark datasets: UCF-HN containing 100 videos, and MSAD-HN comprising 67 videos.

<sup>4</sup>[www.vidu.cn/create/img2video](http://www.vidu.cn/create/img2video)

<sup>5</sup>[github.com/comfyanonymous/ComfyUI](https://github.com/comfyanonymous/ComfyUI)

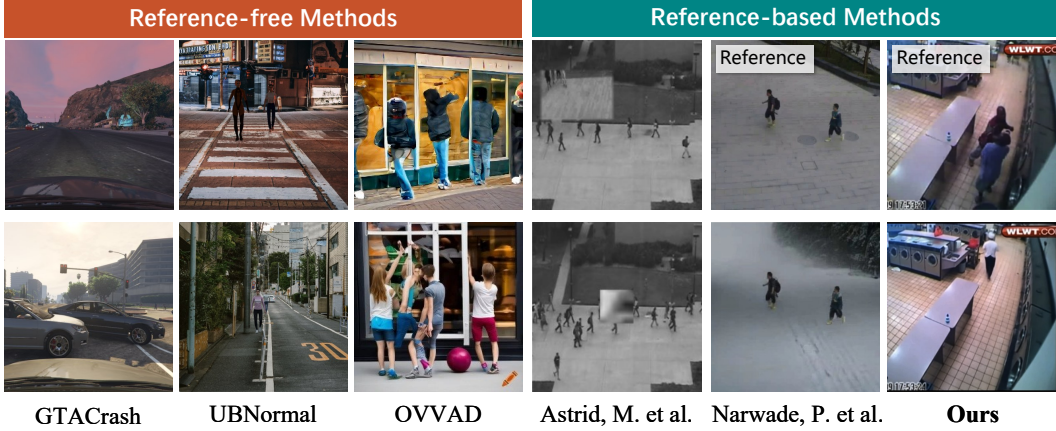


Figure F: Comparisons with other VAD methods using synthetic data [27, 44, 53–55]. Reference-based methods indicate methods that synthesize videos based on existing datasets, while reference-free methods do not rely on existing datasets.

## F.2 Comparisons with other VAD methods using synthetic data.

Figure F presents comparisons with existing synthetic data approaches in VAD. Notably, all compared methods differ in motivation from our work, with the comparison focused solely on generation quality. GTACrash [53] acquires crash data from gaming environments, exhibiting limited physical realism. UBNormal [27] employs 3D modeling software to produce animation, demonstrating suboptimal human motion naturalness and environmental integration. OVVAD [44] employs a text-to-image diffusion model coupled with an image animation model for frame generation, resulting in conspicuous visual artifacts and temporal inconsistencies. Astrid, M. et al. [54] generates anomalies via cut-paste operations, resulting in significant background inconsistency. Narwade, P. et al. [55] synthesizes alternative background states via image-to-image diffusion models while reinserting foreground objects through cut-paste operations, achieving natural motion patterns yet compromised foreground-background integration.

Our work pioneers the application of video diffusion models for benchmark generation, producing data with minimal artifacts, seamless human-environment integration, and unedited temporal continuity. The synthesized videos demonstrate superior realism compared to existing methods.

## F.3 More Visualizations of UCF-HN and MSAD-HN.

We provide more visualizations of our proposed synthetic benchmarks in Figures H,I,J.

## F.4 Discussions of Video Surveillance Data Source.

Current VAD methods primarily focus on surveillance videos. We conduct a systematic discussion on data sources for surveillance video data as follows. The persistent challenge of data scarcity in VAD research is analyzed through four dimensions as in Figure G: **Customizability**, **Realism**, **Scalability**, and **Privacy/Commercial Concern**. Customizability refers to the variety of data you can get from this source; Realism refers to the similarity to real-world scenarios; Scalability refers to the difficulty of obtaining data at scale; Privacy/Commercial Concern addresses legal and commercial restrictions. These four dimensions are the key criteria to measure the quality of a data source.

REAL source denotes authentic surveillance footage containing actual anomaly events, which is typically inaccessible due to privacy constraints. WEB source consists of publicly shared surveillance clips that enable large-scale data collection through crawling.

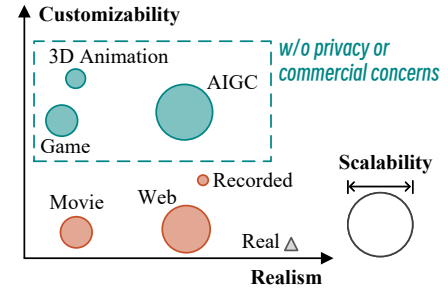


Figure G: Analysis of existing VAD data sources in customizability, realism, scalability, and privacy/commercial concern.



Figure H: Examples of UCF-HN. (a) The original video contains an anomaly of a vehicle hitting an animal. The generated video shows vehicles and bicycles passing normally. (b) The original video contains an anomaly of an explosion. The generated video shows a cleaner walking around.

While being the primary data source for many existing datasets, these videos often suffer from editing and watermarks. Researchers also find it hard to acquire high-quality normal videos, since uploaders generally do not share uninteresting normal surveillance footage. MOVIE source comprises films, TV series, etc., offering visually prominent anomalies (e.g., car crashes, explosions, gunfire) but also containing artistic embellishments that deviate from real-world scenarios. RECORDED source involves staged anomaly simulations, providing controllable environments while inherently the presence of severe real-world anomalies. GAME source leverages interactive virtual spaces and offers flexibility for data acquisition, but its physical simulations and graphical effects may demonstrate discrepancies from reality. 3D ANIMATION source employs mature manual modeling techniques to create synthetic data, achieving higher visual fidelity than game engines by sacrificing real-time rendering capabilities. However, this method demands expertise and labor-intensive production processes. The emerging AIGC source utilizes generative models (e.g., diffusion models) with multimodal control mechanisms (e.g., text prompts, mask images, poses, depth maps). This method demonstrates unique advantages in generating various videos, especially sensitive content (e.g., NSFW, violent), while minimizing human intervention through an automated workflow. Recent advancements in this field promise continuous improvements in realism, customizability, and generation efficiency. Moreover, such synthetic data sources circumvent traditional privacy and commercial limitations.

In conclusion, AIGC represents a promising frontier for VAD research. This paper presents pioneering experiments utilizing AIGC, successfully addressing critical challenges unresolved by conventional data sources.

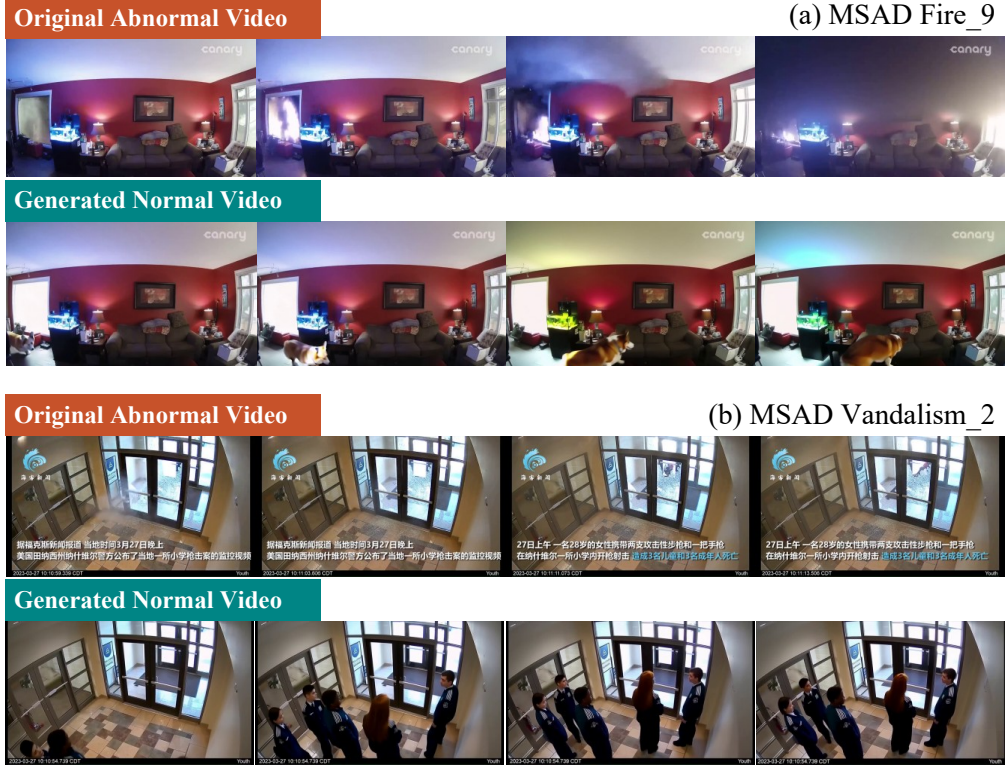


Figure I: Examples of MSAD-HN. (a) The original video contains a fire anomaly. The generated video shows a corgi coming into the room. (b) The original video contains an anomaly involving a glass door being broken. The generated video shows several teenagers talking to each other.

## G Compute Resources

All experiments were performed on a single NVIDIA RTX 4090 GPU, including reproducing baselines, generating videos, and calculating metrics. We did not find an efficient calculation algorithm like AUC/AP as described in [56], however, the computation time on the existing data scale is controlled in the tens of seconds with a consumer-grade CPU.

## H Dataset Statement

**Re-annotations.** Our re-annotations of existing datasets are released exclusively for non-commercial academic purposes, containing no original video content and thereby eliminating potential privacy risks.

**UCF-HN and MSAD-HN.** Our two synthetic benchmarks are based on existing UCF-Crime and MSAD datasets. The generated videos will be released exclusively for academic research or educational purposes. We did not associate the generated content with any real person.

## I Potential Social Impact

This study advances the video anomaly detection field by providing a framework that facilitates the choice of more reliable and timely models, thereby enhancing their implementation in diverse security surveillance architectures. The proposed benchmarks are designed to evaluate if the model overfits on specific confounding elements (e.g., appearance, ethnic characteristics, or scenes), offering a privacy-agnostic evaluation protocol that enhances fairness and safety. This technology could potentially be misused for mass surveillance in combination with other identification technologies.



Figure J: Examples of UCF-HN where multiple videos are generated using the same keyframe. The original video contains a traffic accident anomaly. The generated videos comprise various normal events.